

Equine Trust – Final Report

1. FULL PROJECT TITLE: A novel clinical tool to assess fetlock joint morphology and bone health

2. SHORT TITLE: Assessing fetlock joint morphology and bone health

3. NAME OF ORGANISATION: University of Auckland

4. PROJECT LEADER/CONTACT PERSON: Prof Elwyn Firth,

Department of Exercise Sciences, Faculty of Science,
University of Auckland, PO Box 92019, Auckland 1142
+64 2 74887016
e.firth@auckland.ac.nz

Objective	Description	Completion Date
Objective 1	Create a statistical shape model of the metacarpo-phalangeal joint.	1/4/2016 – Complete
Objective 2	Create a statistical shape model of the fetlock joint to describe its bone mineral density.	30/8/2016 –Complete
Objective 3a	Predict joint morphology and bone mineral density using anthropometric and demographic measurements.	15/12/2016 – Complete
Objective 3b	Write journal manuscript, prepare figures, write paper	30/3/17 – Complete

Objective 1: Create a statistical shape model of the metacarpo-phalangeal joint (MCPJ) capable of reproducing the variation in joint shape to within 2mm RMS error.

Status update: This stage of the project is complete.

Methods overview

Table 1: Subject information on the 40 thoroughbreds used for the study

Age	22 4yo+	11 0-4yo	7 age unknown
Sex	26 female	11 male	3 unknown
Racing history	12 raced	5 unraced	23 unknown

A sample population of 40 left and right MCP joints (Table 1) from slaughtered TB horses was obtained from an abattoir, and used to create a statistical shape model. The MCP joints were scanned using a computed tomography (CT) scanner (140 KV, in plane resolution 0.3 mm, out of plane 0.6 mm, SOMATOM Definition Flash, Siemens Healthcare) (Figure 1a).

Data clouds representing the surfaces of the third metacarpal bone, the proximal phalangeal bone, and the medial and lateral proximal sesamoid bones were segmented from the images using Stradwin (Cambridge University, Cambridge, UK) (Figure 1b).

A single surface data cloud from each bone was chosen as the template joint, and a custom cubic-Lagrange piece-wise parametric mesh was manually created to closely fit the surface. This template mesh was fitted to the remaining data clouds in the training set via an iterative fitting process (Figure 1c).

The fitted meshes were then rigidly aligned to each other by minimizing the least squared distances of corresponding points. The purpose of this process is to create a consistent mesh that accurately represents the segmented point cloud for all specimens. [1, 2]

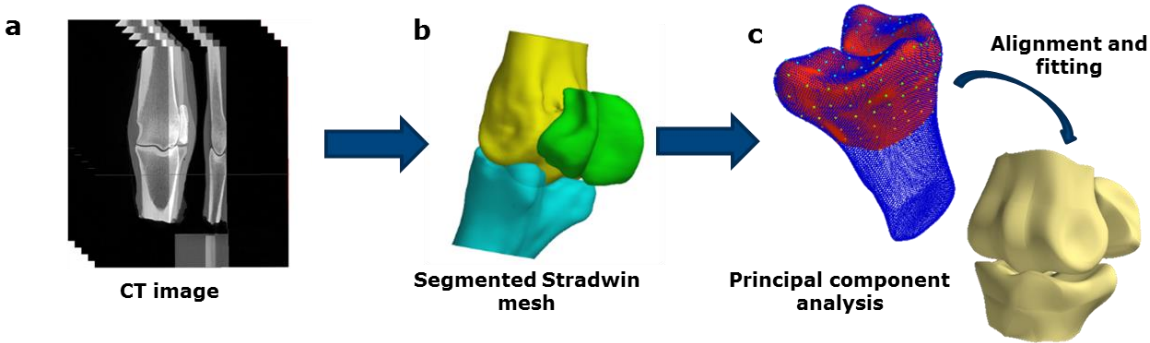


Figure 1: Pipeline for creating the statistical shape model - geometry only.

A Principal Component Analysis, or PCA, was carried out on the mesh node coordinates to obtain a shape model, and determine the principal directions and weights of variation in the population. As size normally dominates the first principal component, a general Procrustes analysis [3, 4] was performed on the data, which is a least squares minimization of correspondent point differences to account for overall size variation.

Results

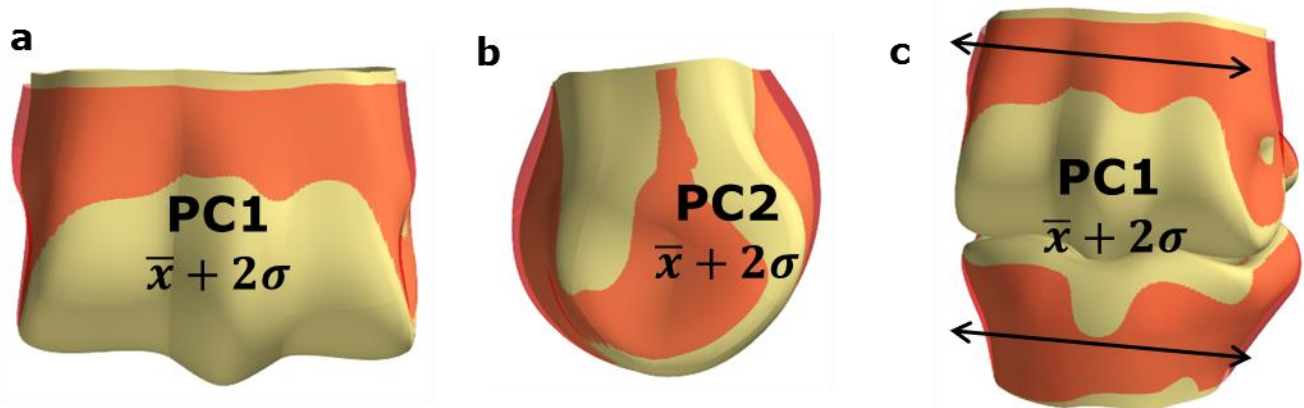


Figure 2: Principal modes of variation. a) The first principal component of the third metacarpal bone, showing the two extremes as solid beige and transparent red, b) second principal component, c) the coupled first principal component of variation for the four bones in the MCPJ.

PCA was used for dimensionality reduction, so that any shape in the training set can be represented by a mean and a weighted sum of principal components.

The first 10 principal components of the size-normalized model accounted for 75% of the variation. There was a noticeable decrease in the gradient of the cumulative variation curve around the third principle component, suggesting that subsequent modes were not uniquely and consistently defined (Figure 3).

Examination of the eigenvalues produced by the PCA showed that the first mode in the size-normalized model contained 27% of the variance in the training set in the left leg, and about 19% of the variance in the right leg. This mode appeared to be dominated by a thickening of the metaphysis, without showing much variance in the articulating surfaces (Figure 2a). The second mode, accounting for about 16 and

12% of the variance in the right and left leg respectively, appeared to describe the height of the sagittal ridge, a feature to which some research has linked

fracture risk (Figure 2b). [5] I also performed a PCA on the coupled shape changes of the four bones making up the MCP joint. The first mode showed a thickening of the metaphyses of the third metacarpal bone and the proximal phalangeal bone, and a thickening of the apex of the sesamoid bones (not visible in the image) (Figure 2c).

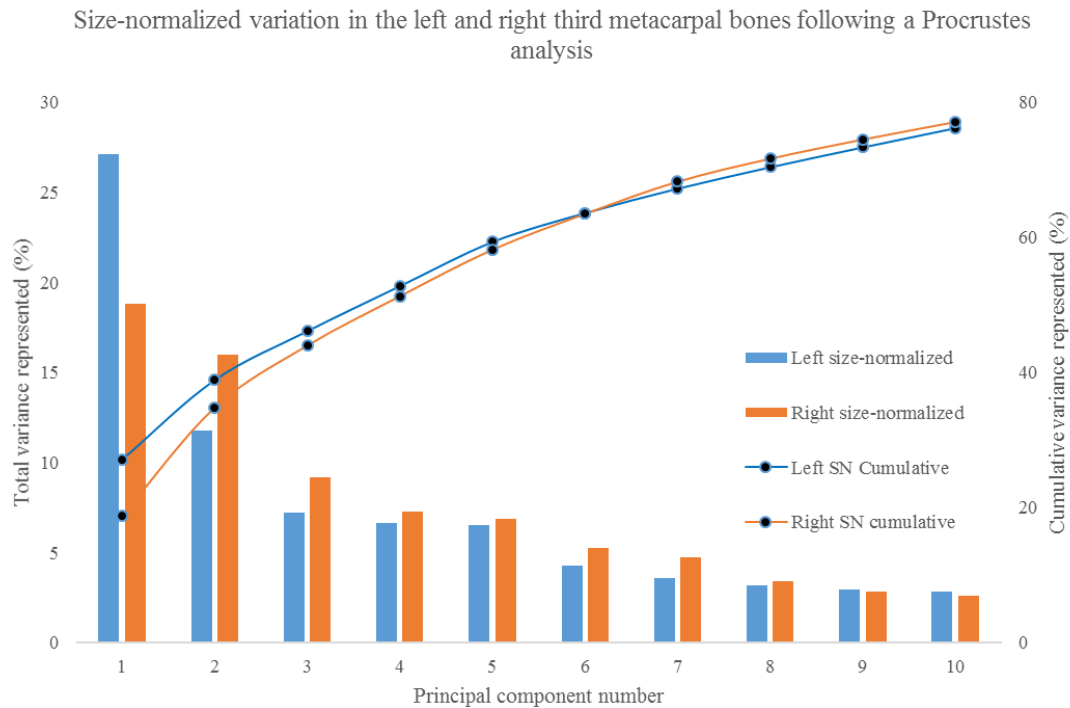


Figure 3: Variation and cumulative variation represented by principal component number in size-normalized models of the left (blue) and right (orange) third metacarpal bones

Conclusion

The fit of the template mesh to each dense surface cloud was accurate to 0.36 mm RMS error, so we are confident in the accuracy of the final population model.

Objective 2: Incorporate bone mineral density into the statistical shape model.

Status update: This stage is complete. We created two correlated shape/BMD statistical shape models for this analysis. Initially we created a high quality tetrahedral mesh of the third metacarpal bone, and fit this to all the other bones using a two-step host mesh fitting process. However, it proved difficult to reduce the dimensionality of this model into meaningful modes, possibly due to the averaging effect of the interior elements. The second model sampled each node on the surface by projecting a normal vector 0.5 mm into the bone and averaging along this vector. Each training example, described by their nodal coordinate positions and modulus value at each node, will then be analysed by PCA using a correlation based approach. [6]

Introduction

The aim of this study was to use a statistical shape and image intensity model to investigate the relationship between the bone shape and the spatial distribution of bone mineral density in the equine third metacarpal bone.

We predicted that the main source of variation will be a scaling of the bone. An increase in size will be correlated to an increase in subchondral bone mineral density (SCB BMD).

Secondly, we hypothesize that variation will be present in the relative area of the metacarpal condyles. It is known that the medial condyle is larger in area and less angled than the lateral condyle [7-9] and also experiences higher load [10-13]. We predict that an increasing ratio of medial to lateral condylar area will be correlated to increased asymmetry in BMD in the bone regions that articulate with the proximal phalangeal and proximal sesamoid bones.

Methods

Overview

To understand the variation in the morphology and bone mineral density of the MCPJ across the population, a statistical model was trained using computed tomography (CT) scans collected from 40 thoroughbred horses. The development of the statistical shape model was based on the methods of Zhang et al. [1] This required establishing correspondence between each specimen so that the location and bone mineral density at any given point in one model can be related to an equivalent point in another model. The workflow describing these steps is illustrated in **Error! Reference source not found.** **Error! Reference source not found.** and described below.

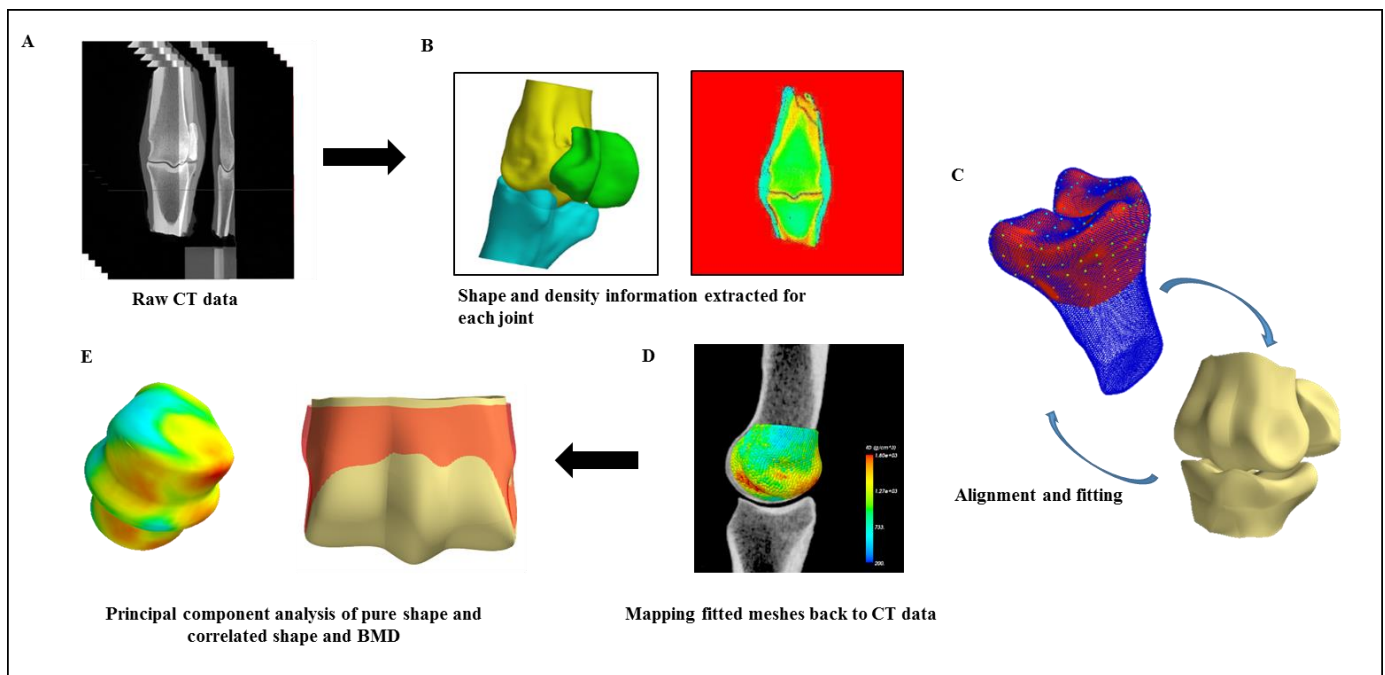


Figure 4: Workflow to generate a statistical shape model of the metacarpo-phalangeal joint using CT imaging data

Specimens

The MCP joints used in this study were from 40 thoroughbred horses sent to the abattoir for reasons unrelated to MCP joint injury. Some information on the horses was obtained from the brands on the shoulder of the animals (Table 1), but on occasion this was unable to be traced, or not visible.

A: Imaging protocol

The left and right MCP joints were bisected proximally at approximately halfway down the MC3, and distally at halfway down the proximal phalangeal bone. The joints were labelled and frozen prior to being transported to the imaging center. The MCP joints were scanned using a Siemens SOMATOM CT scanner (140 KV; in plane resolution 0.3 mm, slice thickness 0.6 mm). The bones were scanned in the same image space as a hydroxyapatite (HA) phantom with a known mineral density of 800mg/mm³.

B: Segmentation and calculation of apparent bone mineral density

Data clouds representing the surfaces of the third metacarpal bone (MC3), the proximal phalangeal bone (PP), and the lateral and medial proximal sesamoid bones (PSB's) were segmented from the CT images using Stradwin (Cambridge University, Cambridge, UK), and constitute the sample population, or "training set".

C: Alignment and fitting

The development of the statistical shape model was based on the methods of Zhang et al. [1]

From the training set, one mesh was chosen as the template, from which a custom template cubic lagrange, piece-wise parametric mesh was created to closely fit the surface. [14] This mesh was subsequently brought into close alignment (<0.5 mm RMS) with each data cloud using host mesh fitting. [2] Following this, a rigid alignment minimized the least squares distances of corresponding points, such that PCA could be performed on the node coordinates to obtain a shape model. [1, 2]

The shape model could then be used to refit the mesh, to decrease the fitting error, and propagate fitting correspondence. This was performed iteratively until the RMS was reduced to <0.3 mm and did not continue to decrease. Finally, a principal component analysis (*Section E*) on the maximally correspondent meshes yielded the principal components of variation in the bone.

Section C.1 Morphometry analysis

MC3 morphometric measurements (Figure 5) were automatically taken on the surface meshes segmented from CT images. As a single correspondent mesh was fitted to each bone during segmentation, each MC3 surface was parameterized by a common coordinate system, allowing anatomical features to be defined by singular nodes (MC3 width, ridge width) or sets of face elements (condylar area/total area). These measurements were used to quantify the variation observed in the model.

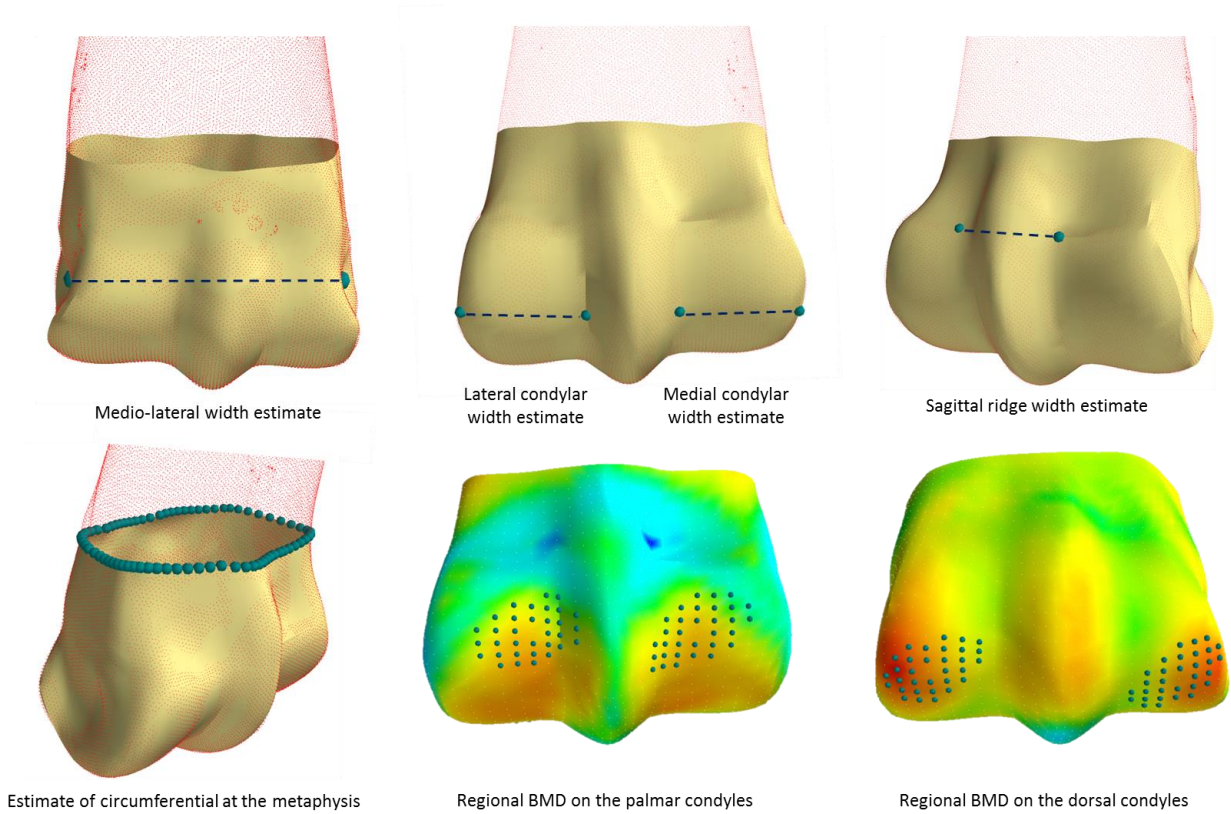


Figure 5 Initial estimates of third metacarpal shape and material parameters to quantify changes observed in the principal component analysis.

D: Mapping fitted meshes back to CT data

Once the surface mesh was fit to the specimen geometry, it was mapped back to the original DICOM files using a custom Python script. At each node location, a vector normal to the surface was projected inwards 5 mm, which is the approximate depth of equine sub-chondral bone affected by exercise. [Brama 2009] The CT data was sampled along this vector, and the average value (Hounsfield Units) was assigned to the node.

The bones were scanned in the same image space as a hydroxyapatite (HA) phantom with a known mineral density of 800mg/mm^3 . Greyscale values were converted from Hounsfield units to apparent bone mineral density with the following equation:

$$r_{HA} = \frac{CT_{bone} - CT_{H_2O}}{CT_{HA} - CT_{H_2O}} \cdot r_{Phantom} \quad (1)$$

Modulus values were calculated by using the empiric relationship described by Dalstra et al [15, 16]:

$$r_{app} = \frac{r_{HA}}{0.626}, E = 2017.3 r_{app}^{2.46} \quad (2)$$

Where ρ_{app} is the apparent bone mineral density (g/cm^3) and ρ_{HA} the HA equivalent density calculated from equation (1).

E: Principal Component Analysis of Shape and Bone Mineral Density

The correspondence between every training example enabled the location and material properties at any given point in the model can be directly related to an equivalent point in another model.

PCA provided a statistical technique to decompose the data in the training set into its significant components. The training dataset was an $N \times 3n$ matrix, where N is the number of geometries in the training set and n is the number of nodes in the mesh. This PCA model allowed any shape x in the training set to be approximated as a sum of the mean shape \bar{x} and the weighted sum of n principal components ϕ . [1]

$$x = \bar{x} + \sum_{i=0}^n \omega_i \phi_i \quad (3)$$

In the model above, to create a new bone instance x , sum the mean of the training geometries \bar{x} , with the product of n included basis vectors with the coefficients controlling their influence (ω_i). N is chosen such that the accumulated variance explained by the components accounted for 80% of the total variation in the population. Singular value decomposition was used to reduce the size of the correlation matrix. [17]

To incorporate bone mineral density, a point distribution model was used. In this case the training dataset was an $N \times 4n$ matrix, containing dimensional data x , y , and z with modulus data I . [6, 18] Jolliffe [19] found that a correlation based PCA approach was more suited to data with mixed units, as here where distance and modulus are present (as opposed to the commonly used covariance approach). This PCA model was able to examine the effect of each principal mode of variation on shape and spatial variability of bone density.

Quantitative analysis

For each principal mode of variation, the joint shape was reconstructed at ± 2 s.d, to represent 95% of the population. Metrics including the total area, the condylar area and the medio-lateral width (Figure 5) were compared to literature and used to quantitatively describe the variation.

Results and Discussion:

Summary

A three dimensional statistical analysis of the third metacarpal bone is presented. The main modes of variation in the shape and bone mineral density distribution are presented individually, and to correlated effect. The purpose of this study was to characterize the size, shape and material properties of the MC3 bones in a cohort of 40 healthy thoroughbred subjects, using a statistical shape model. We characterized morphological differences in the population of third metacarpal bones using a pure shape model, and investigated form-function relationships using a point distribution model which incorporated sub-chondral bone mineral density information at the surface nodes.

Principal Component Analysis

For the PCA conducted on the shape alone, 85% of variation was captured in the first ten principal modes of variance. The BMD field PCA was slightly more compact, covering 89% of variation. The combined shape and BMD PCA accounted for 74% variation in ten modes. As evident in Figure 6, for all models, the first component (size) accounted for most of the variation.

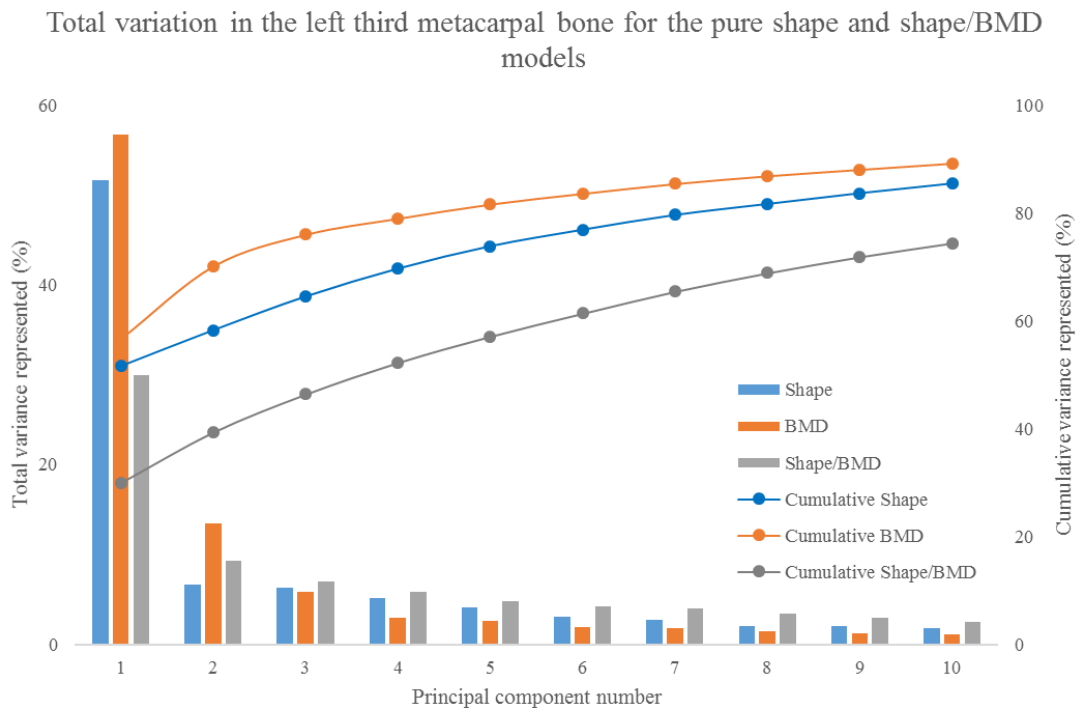
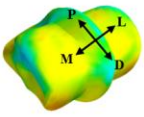
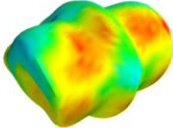
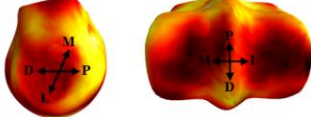
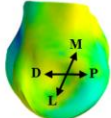
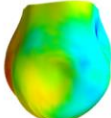
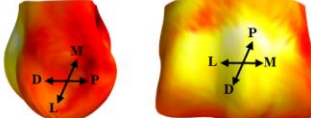
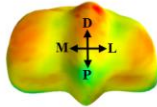
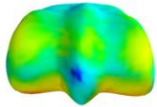
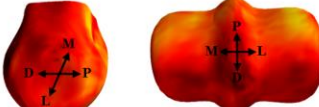


Figure 6 Absolute and cumulative variation for the principal component analysis on shape, BMD and combined shape/BMD models.

The physical effect of each eigenmode on material characteristics was investigated by manipulating each mode in isolation and visualizing the result.

Variation represented by the first three components of the combined PCA model is shown in Table 2. The components respectively represent, (1), positive scaling in overall size with associated SCB BMD increase, (2), increased ridge prominence on the dorsal metaphysis, coupled to increased BMD in that region, and (3), a change in condylar area ratio with associated increased dorsal BMD. These modes of variation matched the variations seen in the first three components of the shape-only and cortical thickness only PCA models.

Table 2 The first three principal components of variation for the correlated shape and bone mineral density PCA on the third metacarpal bone.

Principal Component (% Variance)	-2 SD	+2 SD	Δ BMD over epiphysis (darker red corresponds to greater increase)	Description
1 (30%)				<p>30% increase in total area</p> <p>16% increase in BMD over proximal phalangeal articulation ($1.6\text{--}1.9\text{ g.cm}^{-3}$),</p> <p>10% increase over sesamoid articulation ($1.5\text{--}1.7\text{ g.cm}^{-3}$)</p>
2 (9%)				<p>Observable change in dorsal shape at the metaphysis of the bone.</p> <p>Change in proximal phalangeal articulation BMD ($1.6\text{--}2.0\text{ g.cm}^{-3}$)</p>
3 (7%)				<p>10% increase in lateral condylar size relative to medial condylar size</p> <p>10% increase in proximal phalangeal articulation BMD ($1.7\text{--}1.9\text{ g.cm}^{-3}$)</p>

*M = medial, L = lateral, D = dorsal, P = palmar

Morphological variations

This process of fitting a correspondent mesh to subject-specific geometries from CT can introduce artificial variations into the models. However, the major principal components exhibited expected anatomical variations without any visible geometric abnormalities, suggesting that the model-creation process did not introduce significant noise to metacarpal shape or BMD distribution.

The first component of the shape and cortical thickness combined PCA model described an overall scaling of the bone epiphysis and was coupled to an increase in surface bone mineral density, especially in the regions where the proximal phalangeal bone and proximal sesamoid bones articulate with the MC3. This is an expected result for biomechanical applications of statistical shape models. [1, 2, 6]

The second mode of variation can be qualitatively described as an increased convexity of the dorsal metaphysis. This was coupled to increased BMD at the dorsal extremity of where the proximal phalangeal bone articulates with the MC3 at the gallop.

The third mode of variation, which only accounted for 7% of the total variation, showed a change in lateral condylar area relative to medial condylar area. As the condyle reduced in relative area, the BMD at the dorsal regions increased uniformly across the joint. This was not a sufficiently clear result to support our hypothesis that increased shape asymmetry would correlate to BMD medio-lateral asymmetry.

The influence of the modes provides an insight into how this set of metacarpal bones vary, however these modes will never occur in isolation. Any metacarpal bone in reality will be the product of the combined effect of a number of modes, which may result in the features observed being cancelled out or exaggerated.

Additional statistical analyses are described in the associated articles (Objective 3b) to augment our confidence in the ability of the model to reproduce expected variation (*leave-one-out analysis*), and to ensure the sampled population used was representative.

The immediate next step we have planned for this research is to use these statistical predictions in an existing finite element model. The effect of these shape and material changes on stress distribution throughout the joint may contribute more to this hypothesis.

Objective 3A: Predict joint morphology and bone mineral density using anthropometric and demographic measurements.

Introduction

Finite element methods have been used in equine research to model stresses on the third metacarpal bone [8, 20-22]. Finite element modelling is usually based off data collected from computer tomography (CT) and/or magnetic resonance imaging (MRI). These images create a subject specific model for bone material and geometry. A finite element analysis performed on these models can infer stresses and strains unique to that subject for a range of loading conditions. The validity of these models to then infer fracture and bone disease risk to a different horse is limited, as the mechanical contribution is dependent on of shape and material distribution, which has an unquantified variation across the population.

Finite element models of the Equine fetlock joint are not currently used as a diagnostic tool, due to the difficulty and expense of obtaining diagnostic images from live animals for subject specific models. The goal of this research was to investigate whether basic measurements of bone geometry could be used to predict third metacarpal bone shape using partial least squares regression.

Using anthropological and morphometric data to predict geometry and cortical thickness has been extensively studied in the human femur [1, 23, 24]. Morphometric measurements constrained the predicted geometry and were found to be more successful than anthropological data in predicting shape, reducing the fitting error to less than 2 mm. [1]

This predictive model presents a new way to infer subject-specific 3-D MC3 morphology from sparse subject data for biomechanical simulations

Methods

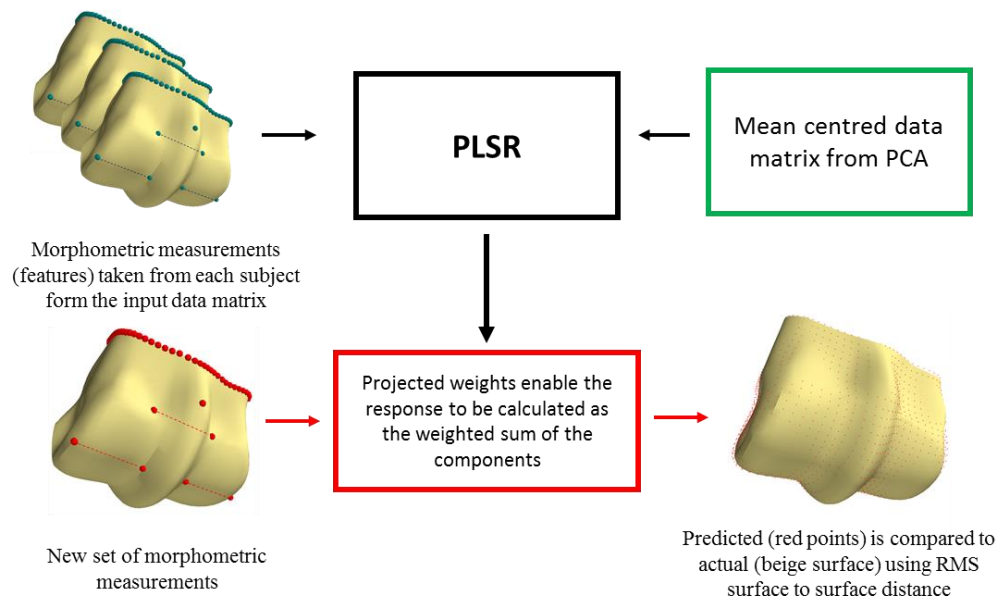


Figure 7 Workflow for partial least squares regression

As described in Objective 2, the MC3 surface in each CT image was automatically segmented and converted into digital 3-D models, on which shape analysis and morphometric measurements were then

performed. MC3 morphometric measurements (Figure 5) were automatically taken on the surface meshes segmented from CT images. As a single correspondent mesh was fitted to each bone during segmentation, each MC3 surface was parameterized by a common coordinate system, allowing anatomical features to be defined by singular nodes (MC3 width, ridge width) or sets of face elements (condylar area/total area).

Principal component analysis (PCA) was performed on the population of MC3 models and BMD was sampled at the surface to model the main modes of variations.

Inverse statistical models for predicting cortical morphology from morphometric data were created using partial least-squared regression (PLSR). For the PLSR, the mean-centered data matrix used for the combined shape and BMD PCA was used as the response matrix. In each model, PLSR was used to find components of maximal covariance between the predictors and the response. During prediction, unseen predictors are projected as weights for the components, which allow the response to be reconstructed as the weighted sum of the components (Figure 7). For shape prediction, RMS surface-to-surface distance was calculated between actual and predicted surfaces. Further detail on inverse statistical models can be found in [1] and [18].

Results and Discussion

Using morphometric measurements, the PLSR was able to recreate third metacarpal bone shape to 1 mm RMS. This was expected as measurements are directly correlated to third metacarpal bone geometry. Qualitatively, most errors in prediction occurred on the metaphysis, with both width and sagittal ridge height in this location underestimated. Prediction accuracy was high over the distal articulating surface of the joint.

The PCA of third metacarpal bone shape produced a less compact model than similar studies on human joints, in which up to 99% of shape and size variation was captured in less than ten significant components. [1, 2, 25] The shape model performed here accounted for 84% of the variation in the first ten modes, with more than 25 modes required to represent 99% variation. The cumulative variation curve (Figure 6) is expected to flatten when the components are no longer uniquely and consistently defined. [2] Increasing the number of predictive weights in the PLSR beyond the first four showed an increase in RMS fitting error, suggesting that those modes only describe noise.

Objective 3B: Submit two journal articles

Two papers have been completed, and are currently being reviewed by the supervisory team.

The first paper, entitled “*Correlated shape and bone mineral density features in the equine third metacarpal bone*” will be submitted to the open access journal PLOS.

The second paper entitled “*Using PLSR as a predictive tool in describing third metacarpal bone shape*” is a technical paper on the use of partial least-squared regression in predicting third metacarpal epiphyseal shape.

Conference Abstracts:

Liley, H., Firth, E., Fernandez, J., Besier, T., Zhang, J. (2016) “Shape variation in the equine metacarpophalangeal (fetlock) joint” *European Society of Biomechanics Annual Congress, Lyon, France*

Liley, H., Besier, T., Firth, E., Davies, H., Fernandez, J. (2015) “Age-related shape characteristics in the equine fetlock joint” *Australia and New Zealand Orthopaedic Research Society Annual Meeting, Auckland, NZ*

References

1. Zhang, J., et al., *An anatomical region-based statistical shape model of the human femur*. Computer Methods in Biomechanics and Biomedical Engineering: Imaging & Visualization, 2014. **2**(3): p. 176-185.
2. Schneider, M.T., et al., *Men and women have similarly shaped carpometacarpal joint bones*. J Biomech, 2015. **48**(12): p. 3420-6.
3. Bischoff, J.E., et al., *Incorporating population-level variability in orthopedic biomechanical analysis: a review*. J Biomech Eng, 2014. **136**(2): p. 021004.
4. Ross, A., *Procrustes Analysis*. 2004, Department of Computer Science and Engineering, University of South Carolina, South Carolina (2004).
5. Alrtib, A.M., *Fetlock joint angle in equine forelimbs*. Proceedings of the Australian Veterinary Association. Vol. 2011 AVA Annual Conference. 2011: Australian Veterinary Association.
6. Bryan, R., et al., *Statistical modelling of the whole human femur incorporating geometric and material properties*. Medical Engineering & Physics, 2010. **32**(1): p. 57-65.
7. Yoshihara, T., et al., *An application of the image analyzer to the soft radiogram of the third metacarpus in horses*. Nihon Juigaku Zasshi, 1989. **51**(1): p. 184-6.
8. Easton, K., *Effect of bone geometry on stress distribution patterns in the equine metacarpophalangeal joint*, in *Bioengineering*. 2012, Colorado State University: Fort Collins.
9. Alrtib, A.M., et al., *Morphometrical study of bony elements of the forelimb fetlock joints in horses*. Anat Histol Embryol, 2013. **42**(1): p. 9-20.
10. Santschi, E.M., et al., *Carpal and fetlock conformation of the juvenile Thoroughbred from birth to yearling auction age*. Equine Vet J, 2006. **38**(7): p. 604-9.
11. Firth, E.C., H.C. Schamhardt, and W. Hartman, *Measurements of bone strain in foals with altered foot balance*. Am J Vet Res, 1988. **49**(2): p. 261-5.
12. Boyde, A., et al., *Three dimensional structure of the distal condyles of the third metacarpal bone of the horse*. Equine Vet J, 1999. **31**(2): p. 122-9.
13. Riggs, C.M. and A. Boyde, *Effect of exercise on bone density in distal regions of the equine third metacarpal bone in 2-year-old thoroughbreds*. Equine Vet J Suppl, 1999. **30**: p. 555-60.
14. Nielsen, P.M.F., *The Anatomy of the Heart: A Finite Element Model*, in *ResearchSpace@Auckland*. 1987: Auckland.
15. Dalstra, M., et al., *Mechanical and textural properties of pelvic trabecular bone*. J Biomech, 1993. **26**(4-5): p. 523-35.
16. McKellop, H., et al., *Wear characteristics of UHMW polyethylene: a method for accurately measuring extremely low wear rates*. J Biomed Mater Res, 1978. **12**(6): p. 895-927.
17. Golub, G., Van Loan, C. , *Matrix Computations*. 1996, The John Hopkins University Press.
18. Cootes, T.F., et al., *Active Shape Models-Their Training and Application*. Computer Vision and Image Understanding, 1995. **61**(1): p. 38-59.
19. Jolliffe, I., *Principal Component Analysis*. 2002, Wiley Online Library.
20. Harrison, S.M., et al., *Evaluation of a subject-specific finite-element model of the equine metacarpophalangeal joint under physiological load*. Journal of Biomechanics, 2014. **47**(1): p. 65-73.

21. McCarty, C.A., et al., *Finite-Element Analysis of Bone Stresses on Primary Impact in a Large-Animal Model: The Distal End of the Equine Third Metacarpal*. PLoS One, 2016. **11**(7): p. e0159541.
22. Les, C.M., et al., *Estimation of Material Properties in the Equine Metacarpus with use of Quantitative Computed Tomography*. Journal of orthopaedic research : official publ. of the Orthopaedic Research Society and the Bioelectric Repair and Growth Society, 1994. **12**(6): p. 822-833.
23. Blanc, R., et al., *Statistical model based shape prediction from a combination of direct observations and various surrogates: application to orthopaedic research*. Med Image Anal, 2012. **16**(6): p. 1156-66.
24. Serrurier, A., et al., *Distribution and variability study of the femur cortical thickness from computer tomography*. Comput Methods Biomech Biomed Engin, 2014. **17**(7): p. 768-86.
25. van de Giessen, M., et al., *Statistical descriptions of scaphoid and lunate bone shapes*. J Biomech, 2010. **43**(8): p. 1463-9.